Phase-field study on geometry-dependent migration behavior of voids under temperature gradient in UO_2 crystal matrix

Weijin Chen, Yuyi Peng, Xu'an Li, Kelang Chen, Jun Ma, Lingfeng Wei, Biao Wang, and Yue Zheng

Citation: Journal of Applied Physics **122**, 154102 (2017); doi: 10.1063/1.4996692
View online: https://doi.org/10.1063/1.4996692
View Table of Contents: http://aip.scitation.org/toc/jap/122/15
Published by the American Institute of Physics

Articles you may be interested in

Temperature induced phase transformations and negative electrocaloric effect in (Pb,La)(Zr,Sn,Ti)O_3 antiferroelectric single crystal
Journal of Applied Physics **122**, 154101 (2017); 10.1063/1.4986849

Advanced MOKE magnetometry in wide-field Kerr-microscopy
Journal of Applied Physics **122**, 153906 (2017); 10.1063/1.5003719

Grain-size dependent electric-field induced structural changes and its role in determining the piezoelectric response of 0–3 piezoceramic-polymer composite
Journal of Applied Physics **122**, 154105 (2017); 10.1063/1.5000127

Reconfigurable origami sonic barriers with tunable bandgaps for traffic noise mitigation
Journal of Applied Physics **122**, 154901 (2017); 10.1063/1.4991026

The critical electric field of gas mixtures over the extended range of cryogenic operating conditions
Journal of Applied Physics **122**, 153301 (2017); 10.1063/1.4995663

Influence of tetragonality (c/a) on dielectric nonlinearity and direct current (dc) bias characteristics of (1-x)$BaTiO_3$-x$Bi_{0.5}Na_{0.5}TiO_3$ ceramics
Journal of Applied Physics **122**, 154103 (2017); 10.1063/1.5000019

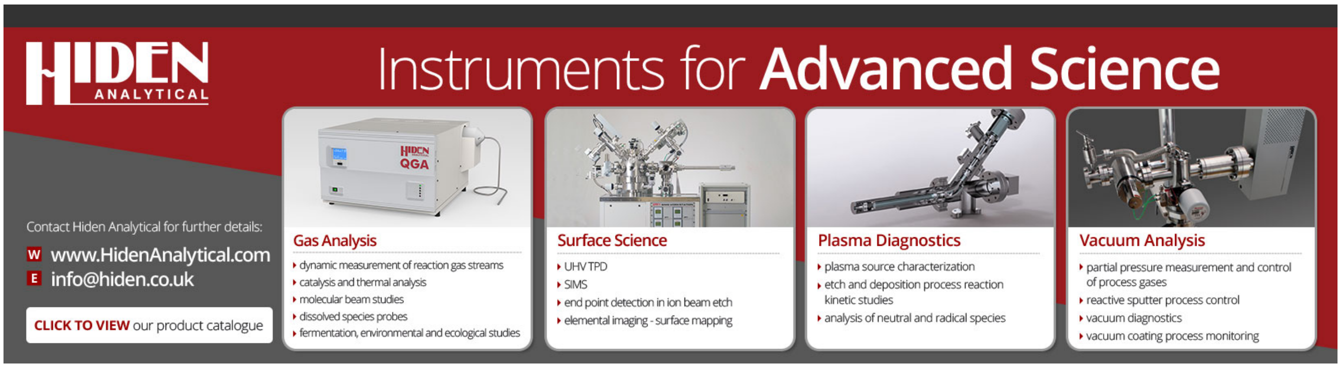

HIDEN ANALYTICAL

Instruments for **Advanced Science**

Contact Hiden Analytical for further details:
W www.HidenAnalytical.com
E info@hiden.co.uk

CLICK TO VIEW our product catalogue

Gas Analysis
- dynamic measurement of reaction gas streams
- catalysis and thermal analysis
- molecular beam studies
- dissolved species probes
- fermentation, environmental and ecological studies

Surface Science
- UHV TPD
- SIMS
- end point detection in ion beam etch
- elemental imaging - surface mapping

Plasma Diagnostics
- plasma source characterization
- etch and deposition process reaction kinetic studies
- analysis of neutral and radical species

Vacuum Analysis
- partial pressure measurement and control of process gases
- reactive sputter process control
- vacuum diagnostics
- vacuum coating process monitoring

JOURNAL OF APPLIED PHYSICS **122**, 154102 (2017)

Phase-field study on geometry-dependent migration behavior of voids under temperature gradient in UO_2 crystal matrix

Weijin Chen,[1,2,3] Yuyi Peng,[2,3,4] Xu'an Li,[1] Kelang Chen,[1] Jun Ma,[1] Lingfeng Wei,[1]
Biao Wang,[1,a)] and Yue Zheng[2,3,b)]
[1]*Sino-French Institute of Nuclear Engineering and Technology, Sun Yat-sen University, Zhuhai 519082, China*
[2]*State Key Laboratory of Optoelectronic Materials and Technologies, Sun Yat-sen University, 510275 Guangzhou, China*
[3]*Micro&Nano Physics and Mechanics Research Laboratory, School of Physics, Sun Yat-sen University, 510275 Guangzhou, China*
[4]*Shenzhen Key Laboratory of Advanced Materials, Shenzhen Engineering Lab of Flexible Transparent Conductive Films, Department of Materials Science and Engineering, Shenzhen Graduate School, Harbin Institute of Technology, Shenzhen 518055, China*

(Received 18 July 2017; accepted 3 October 2017; published online 17 October 2017)

In this work, a phase-field model is established to capture the void migration behavior under a temperature gradient within a crystal matrix, with an appropriate consideration of the surface diffusion mechanism and the vapor transport mechanism. The interfacial energy and the coupling between the vacancy concentration field and the crystal order parameter field are carefully modeled. Simulations are performed on UO_2. The result shows that for small voids (with an area $\leq \pi\mu m^2$), the well-known characteristics of void migration, in consistence with the analytical model, can be recovered. The migration is manifested by a constant velocity and a minor change of the void shape. In contrast, for large voids (with an area of $\sim 10\ \mu m^2$) initially in circular shapes, significant deformation of the void from a circular to cashew-like shape is observed. After long-time migration, the deformed void would split into smaller voids. The size-dependent behavior of void migration is due to the combined effect of the interfacial energy (which tends to keep the void in circular shape) and the surface diffusion flow (which tends to deform the void due to the nonuniform diffusion along the surface). Moreover, the initial shape of the void modifies the migration velocity and the time point when splitting occurs (for large voids) at the beginning of migration due to the shape relaxation of the void. However, it has a minor effect on the long-time migration. Our work reveals novel void migration behaviors in conditions where the surface-diffusion mechanism is dominant over the vapor transport mechanism; meanwhile, the size of the void lies at a mediate size range. *Published by AIP Publishing.* https://doi.org/10.1063/1.4996692

I. INTRODUCTION

Microstructure evolutions, such as the formation of point defects and defect clusters caused by displacement collision cascades,[1–3] growth, migration, and coalescence of voids and bubbles driven by the diffusion and redistribution of vacancies, interstitials and gas atoms,[4–9] grain growth due to the high temperature sintering effect,[10–12] as well as phase-separation and precipitation,[13–15] etc., are commonly observed in nuclear materials during irradiation. Occurring at length scales spanning from the atomistic scale to the continuum scale and at time scales spanning from several picoseconds to dozen of years, these microstructure evolutions together play crucial roles in determining the overall performance of the nuclear fuels and cladding materials. In particular, it is well-known that the microstructures strongly affect the material properties such as the thermo-mechanical properties (e.g., thermal conductivity, ductility, and creep properties) and can lead to structural instabilities such as swelling and cracking as well as product gas release.[16–20] It is of both fundamental and engineering significance to first gain an in-depth understanding of the characteristics of microstructural changes in irradiated materials, for further modeling and optimizing the performance of nuclear reactor components.

At normal working conditions, there is a large temperature gradient in the nuclear fuel rods. In particular, in fuel materials with a low thermal conductivity, e.g., uranium dioxide UO_2, the center region temperature is above 2000 °C whereas the edge region temperature is about 400–500 °C. This great temperature gradient drives the voids to migrate towards the center of the fuel rod, and causes the formation of a central cavity and the densification of the fuel material.[21,22] During their migration, voids can capture the reaction product gas, and bring it to large cracks or to the central cavity. Thus, void migration plays an important role in gas release. Nonuniform grain coarsening in the fuel rods also happens due to the large temperature gradient. Due to the interaction between voids and grains, void migration can play an important role in grain coarsening, and conversely, the crystalline structure also affects the void migration behavior.[12,23–26] With the deepening of fuel consumption, deformation of the fuel rods and gas release become more and more serious under the combined effects of void

---

[a)] Electronic address: wangbiao@mail.sysu.edu.cn
[b)] Author to whom correspondence should be addressed: zhengy35@mail.sysu.edu.cn

migration, grain coarsening, and cracking due to the large thermal stress. The gas release further raises the fuel rod internal pressure and causes volume swelling problem.

Migration of voids through a solid essentially requires the transfer of atoms from the leading surface to the trailing surface. It is now known that three mechanisms are possible to cause void migration: bulk diffusion where atoms or vacancies nearby the void surface diffuse in the solid matrix, surface diffusion where atoms or vacancies diffuse along the surface of voids, and vaporization/condensation in which the matrix material vaporizes at the leading surface and condenses at the trailing surface via the vapor phase. In general, the contributions of different mechanisms to the void migration are strong functions of the void size and shape. Migration velocity of voids in regular shapes (e.g., flat, cubic, and spherical shapes) as a function of void size can be captured by analytical models.[27–31] Nevertheless, during the migration, the size and shape of the void can be changed significantly, for example, due to the capture of defect clusters, the initially unstable size and shape caused by the insufficient sintering, and the nonuniform feature of the diffusion flow. At present, a comprehensive understanding of the void migration behavior, especially the size/shape changes of the void during migration, and how such size/shape changes affect the void migration velocity, is still lacking.

From the basic picture of void deformation during thermal migration, there are two important factors that determine the void deformation: the diffusion flow (which tends to deform the void) and the interfacial energy (which tends to keep the void in circular shape). On one hand, the importance of interfacial energy decreases with the increase of void size; thus, voids can deform into non-circular shapes by diffusion flow when the size of the void is above a critical value. On the other hand, the contributions of different mechanisms to the diffusion flow vary with the size of the void. Considering the different spatial features of the diffusion flow caused by different mechanisms, various void deformation behaviors are expected during thermal migration at different size ranges. In the literature, so far only those small enough voids (which would remain in circular shape during migration and the migration is caused by bulk/surface diffusion mechanisms) and large enough voids (which tend to remain in lenticular shape during migration and the migration is dominated by the vapor transport mechanism) have been revealed.[9,26–36] We postulate that there might be a mediate size range where the void can be deformed into non-circular shapes during migration by the surface-diffusion mechanism rather than the vapor transport mechanism. At this mediate size range, there might be interesting but overlooked void deformation behaviors during thermal migration. This postulation should be generally plausible for materials that possess a not too large interfacial energy so that the critical size of void deformation is smaller than the critical size between surface-diffusion and vapor transport mechanisms.

The phase-field method has been proved to be a powerful simulation tool in the mesoscale. Based on a diffuse interface model, the phase-field method has been extensively applied to predict microstructures and their evolution kinetics in various materials processes.[37,38] Recently, phase-field models have also been developed to capture gas bubble and void evolution in nuclear materials.[6–9,12,23,24,26,34–36] The major objective of this work is to develop a phase-field model to make quantitative predictions on the void migration behavior under a temperature gradient in a crystal matrix, and apply it to a realistic system UO_2. To achieve this, we appropriately consider the surface diffusion mechanism and the vapor transport mechanism. The interfacial energy and the coupling between the vacancy concentration field and the crystal order parameter field are carefully modeled. It would be shown that the significant shape change and even splitting behavior can be involved in the migration of the void, which would consequently modify the void migration velocity. Such behaviors depend on the size and initial shape of the void, and are attributed to the combined effect of the interfacial energy and the surface diffusion flow. Similarity between the void migration in the solid and the air bubble rising in the fluid caused by the incompressible two-phase flow is also discussed.

II. MODEL AND METHODOLOGY

A. Phase-field model

In the phase-field model, the conserved vacancy concentration field, c_v, which is in the range of zero to one, is chosen to represent the voids within a solid matrix. It is equal to one in the voids and equals to zero in the matrix. The grains are represented by non-conserved order parameters, η_α, with index α ranging from one to P, and P being the number of grain orientations. η_α are also in the range of zero to one, and take the value of one within a designed grain and zero in other grains or in the voids. By taking into account the bulk free energy and the gradient energy, the free energy functional of the system has the form

$$F = \int \left[f(c_v, \eta_\alpha) + \frac{1}{2}\kappa_v |\nabla c_v|^2 + \frac{1}{2}\sum_{\alpha=1}^{P} \kappa_{\eta\alpha} |\nabla \eta_\alpha|^2 \right] d^3r, \quad (1)$$

where the first term is the bulk free energy density, and the latter two terms are the gradient energy densities for the vacancy concentration field and the grain order parameters. κ_v and $\kappa_{\eta\alpha}$ are the gradient energy coefficients for c_v and η_α, respectively. The coupling between the vacancy concentration field and the grain order parameter field modifies not only the free energy of the system but also affects the evolution equations of the two fields. The form of the bulk free energy density needs to be cautiously chosen. Based on the idea of previous studies,[23,24,39,40] we constructed the following Landau-type of the bulk free energy density

$$f(c_v, \eta_\alpha) = B{c_v}^2(1 - c_v)^2 + C\left\{ \left[3\left(\sum_\alpha \eta_\alpha^2 + {c_v}^2 \right)^2 - 4\left(\sum_\alpha \eta_\alpha^3 + {c_v}^3 \right) + 1 \right] \right\}, \quad (2)$$

where B and C are constants with positive values. Using a similar procedure of previous studies,[23,24,39,40] that is by investigating the equilibrium profiles of the phase fields across flat interfaces, one can derive that B, C, together with κ_v and $\kappa_{\eta\alpha}$ are directly related to material properties as follows:

$$\gamma^{gb} = \frac{2}{\sqrt{3}}\sqrt{C\kappa_\eta}, \tag{3a}$$

$$\gamma^{s} = \frac{1}{6}\sqrt{2(\kappa_v + \kappa_\eta)(B + 12C)}, \tag{3b}$$

$$l = \sqrt{\frac{4\kappa_\eta}{3C}} = \delta, \tag{3c}$$

$$\frac{B + 6C}{\kappa_v} = \frac{6C}{\kappa_\eta}, \tag{3d}$$

where γ^{gb}, γ^{s}, and δ are the grain boundary energy, void surface energy, and grain boundary width, respectively, and l is the diffuse interface width. Note that the form of this bulk free energy density is the same with that used in previous studies,[23,24,39,40] but with a slightly different coupling term between the concentration field and the grain order parameter fields. It can be readily seen that when c_v equals to one, namely in the void phase, the equilibrium values of η_α must be zero. This guarantees the free energy density of Eq. (2) suitable to capture the growth and migration behaviors of voids within the crystal matrix, where the concentration field dominates the overall microstructure evolution.

The evolution of the vacancy concentration field obeys the continuity equation

$$\frac{\partial c_v}{\partial t} = -\nabla \cdot \mathbf{J}, \tag{4}$$

where t is the time and $\mathbf{J}$ is the total vacancy flow density. Taking into account the flow of atomic species caused by the temperature gradient, $\mathbf{J}$ is composed of three terms,

$$\mathbf{J} = -\mathbf{M}\nabla\psi + \mathbf{J}_T + \mathbf{J}_P, \tag{5}$$

where $\mathbf{M}$ is the chemical mobility tensor, ψ is the generalized chemical potential, $\mathbf{J}_T$ is the atomic flow density caused by the thermal transport (i.e., Soret effect) due to the temperature gradient, and $\mathbf{J}_P$ is the flow density of UO_2 molecule vapor caused by the vapor transport mechanism due to the temperature gradient. The generalized chemical potential is given by

$$\psi = \frac{\delta F}{\delta c_v} = \frac{\partial f}{\partial c_v} - \kappa_v \nabla^2 c_v. \tag{6}$$

For a system that comprises of different species, e.g., vacancies and matrix atoms, the temperature gradient can lead to a material transport flow due to the different responses of species to the temperature gradient force. Based on the irreversible thermodynamics, the thermal transport flow density $\mathbf{J}_T$ is given by[31]

$$\mathbf{J}_T = -\frac{\mathbf{M}Qc_v}{T}\nabla T, \tag{7}$$

where T is the temperature and Q is the transport heat.

The temperature gradient also causes a nonuniform vapor pressure distribution at the void surface. As a result, the vaporization/condensation processes of the matrix material at the void surface are also nonuniform, which leads to a nonzero transport flow of the matrix material in the void. The vapor transport flow density $\mathbf{J}_P$ is given by[30]

$$\mathbf{J}_P = -\frac{D_g v_m}{RT}\nabla P_{\mathrm{vap}}, \tag{8}$$

where P_{vap} is the vapor pressure, D_g is the gaseous diffusion coefficient of matrix species in the void, v_m is the molar volume, and R is the universal gas constant.

The gaseous diffusion coefficient D_g is a function of the temperature and the total pressure.[33] Assume that the gas in the void is sintering gas (e.g., Helium). Taking the condition $T = 2000$ K and $P = 1$ atm as the reference state, D_g can be estimated by the following equation:

$$D_g = D_g^*\left(\frac{T}{2000}\right)^{3/2}\left(\frac{1}{P}\right), \tag{9}$$

where D_g^* is the value of the gaseous diffusion coefficient of UO_2 molecule vapor at condition $T = 2000$ K and $P = 1$ atm. The total pressure in the void can be related to the sintering temperature T_{sint} and the sintering pressure P_{sint} as

$$P = \frac{T}{T_{\mathrm{sint}}}P_{\mathrm{sint}}. \tag{10}$$

Note that the mean free path of UO_2 molecules in He gas at $P = 1$ atm and $T = 2000$ K is estimated to be about 700 nm, which is smaller but not too far from the smallest void size we investigated. There is a chance that the vapor transport of UO_2 molecules is ballistic rather than diffusive, especially considering the curvature of the surface. Nevertheless, at this void size range we investigated, the void migration is mainly caused by the surface-diffusion flow rather than the vapor transport flow. Considering the fact that the role of vapor transport becomes less important at small voids, a rough estimation of the vapor transport flow by the use of formulas for the diffusive regime for small voids would not alter the major features of void migration.

The chemical mobility tensor is given by

$$\mathbf{M} = \frac{v_m \mathbf{D}}{RT}, \tag{11}$$

where $\mathbf{D}$ is the diffusion coefficient tensor.

Note that surface diffusion is tangential to the surface; the diffusion coefficient must be expressed as a tensor projecting mass transport onto the surface. This diffusion coefficient tensor can be constructed in a way that is consistent with the sharp interface limit. The expression for the surface diffusion coefficient tensor has the form[23,24,39,40]

$$\mathbf{D}^S = D^S(c_v - 1)^2 c_v^2 \mathbf{T}^S, \tag{12}$$

where D^S is the surface diffusivity and $\mathbf{T}^S$ is the surface projection tensor to guarantee that the surface diffusion is confined along the surface. $\mathbf{T}^S$ is related to the dyadic product of the unit normal to the surface $\mathbf{n}_S = \nabla c_v / |\nabla c_v|$ as

$$\mathbf{T}^S = \mathbf{I} - \mathbf{n}_S \otimes \mathbf{n}_S, \tag{13}$$

with $\mathbf{I}$ being the identity tensor. The function $(c_v - 1)^2 c_v^2$ confines that mechanism to the (diffuse) surface region. It would be shown that the surface diffusion tensor $\mathbf{D}^S$ thus constructed projects the diffusion flow along the void surface, and can cause significant geometry change of the voids during migration.

Moreover, the lattice diffusion tensor is constructed as

$$\mathbf{D}^b = D^b \xi(c_v)\mathbf{I}, \tag{14}$$

where $\mathbf{D}^b$ is the bulk diffusion tensor, D^b is the bulk diffusion coefficient of the matrix material, and $\xi(c_v)$ is a function that confines nontrivial values of diffusivity in the solid region and zero values in the voids.[23] The total diffusion tensor is

$$\mathbf{D} = \mathbf{D}^b + \mathbf{D}^S. \tag{15}$$

Note that, in this work, we consider the void migration within a single crystal matrix. For void migration in a polycrystalline matrix, the grain diffusion tensor can be readily added to the total diffusion tensor.

The kinetic equations of grain order parameters are

$$\frac{\partial \eta_\alpha}{\partial t} = -L\frac{\delta F}{\delta \eta_\alpha} = -L\left(\frac{\partial f}{\partial \eta_\alpha} - \kappa_\eta \nabla^2 \eta_\alpha\right), \tag{16}$$

where L is the kinetic coefficient related to the grain mobility[24]

$$L = \gamma^{gb} M_b / \kappa_\eta, \tag{17}$$

with M_b being the grain mobility.

B. Equations of temperature and pressure fields

The voids, which are usually filled with sintering gas (e.g., He) and product gas (e.g., Xe), generally have a much lower thermal conductivity than that of the matrix.[9,30] Such a difference between the thermal conductivity of the matrix and the voids can strongly modify the temperature field distribution. To take into account this effect, we need to solve the temperature field according to the heat conduction equation. Assume that the system immediately reaches a steady heat conduction state once the concentration field and the grain order fields change. The following steady-state heat conduction equation is used:[9]

$$\nabla \cdot \left(\kappa(c_v)\nabla T\right) + q\left(1 - c_v^2\right) = 0, \tag{18}$$

where q is the heat source constant and $\kappa(c_v)$ is the thermal conductivity which varies spatially according to different phases. The term, $(1 - c_v^2)$, in the heat source term guarantees that no heat is generated within the void. The thermal conductivity $\kappa(c_v)$ is assumed to have the following form:

$$\kappa(c_v) = (\kappa_{\mathrm{void}} - \kappa_{\mathrm{matrix}})c_v + \kappa_{\mathrm{matrix}}. \tag{19}$$

That is, the thermal conductivity in the interfacial zone is linearly interpolated based on the thermal conductivity of the matrix material κ_{matrix} and that of the voids κ_{void}.

Under steady state conditions, the flow density $\mathbf{J}_P$ caused by the vapor transport mechanism in Eq. (8) satisfies the continuity equation,[30] that is

$$\nabla \cdot \left(\frac{D_g v_m}{RT} \nabla P_{\mathrm{vap}}\right) = 0. \tag{20}$$

This elliptical differential equation is similar to the steady heat conduction equation, and it is solved within the void for a given boundary condition of the vapor pressure at the void surface.

The vapor pressure at the void surface is given by[41]

$$P_{\mathrm{vap}}^0 = 10^5 \exp\left(\frac{\Delta S_{\mathrm{vap}}}{k}\right)\exp\left(-\frac{\Delta H_{\mathrm{vap}}}{kT}\right), \tag{21}$$

with ΔS_{vap} and ΔH_{vap} being the vaporization heat and enthalpy, respectively.

C. Numerical implementation

In this work, we focus on the void migration behavior driven by a temperature gradient within a UO_2 single crystal matrix although the model itself is suitable to capture the void migration behavior within a polycrystalline matrix. Void migration in a polycrystalline matrix will be shown in a later work. Simulations are performed on two-dimensional mesh grids. As shown later, the model captures well the basic features of void migration, in consistence with those predicted by three dimensional analytical models. The major conclusions found in our two-dimensional simulations could be extended to real migration of three dimensional voids. In solving the kinetic equations of the concentration field and grain order fields, i.e., Eqs. (4) and (16), a second-order centered finite difference approximation is utilized for all spatial derivatives and an explicit Euler scheme is used for time derivatives. At each time step, the temperature and vapor pressure fields are updated by solving the steady state heat conduction equation and the vapor pressure equation, i.e., Eqs. (18) and (20), *via* a Gauss–Seidel iteration scheme. The vapor pressure is solved within the void. A contour line with $c_v = 0.8$ is used to define the void surface.

For UO_2 with a surface energy of 0.6 J/m^2, a grain boundary energy of 0.3 J/m^2 and a grain boundary width of about nanometers,[24,42] the free energy parameters take on the following values: $B = 1.3585 \times 10^9$ J/m^3, $C = 1.128 \times 10^8$ J/m^3, $\kappa_\eta = 6 \times 10^{-10}$ J/m, and $\kappa_v = 1.8 \times 10^{-9}$ J/m. To make mesoscale simulations, we adopt a diffuse interface which has a width l_0 of about 500 nm instead of the sharp interface while keeping the surface and grain boundary energies invariant.[24] This is achieved by decreasing the values of B and C and decreasing the values of κ_η and κ_v by a factor $N = 187$. In all cases, a 200 × 100 finite difference grid is used. The grid size is taken to be $0.2l_0$ for large voids and $0.1l_0$ for small voids, so that the interface includes at least five mesh points. The values of the diffusion coefficients are taken to be $D_g^* = 1.1 \times 10^{-3}$ m^2/s,[43] $D_s = 50\exp(-450{,}000/RT)$m^2/s,[42] and $D_b = 4 \times 10^{-7}\exp(-290{,}000/RT)$m^2/s.[44] For vaporization of UO_2 molecules, values of the vaporization heat and enthalpy are taken to be: $\Delta S_{vap} = 150\,\mathrm{J\,mol^{-1}\,K^{-1}}$ and $\Delta H_{vap} = 567\,\mathrm{kJ/mol}$.[41] The value of transport heat is $Q = 1.8367 \times 10^{10}\,\mathrm{J/m^3}$.[9] Moreover, the sintering temperature T_{sint} and the sintering pressure P_{sint} are taken to be $T_{sint} = 2000\,\mathrm{K}$ and $P_{sint} = 1\,\mathrm{atm}$. In defaulted simulations, the void is assumed to be filled with helium gas. The conductivity of the void is taken to be 1/5th of that of the UO_2 matrix.[30] The discrete time step is taken to be $6.3 \times 10^{-5}\,\mathrm{s}$, and a maximum number of step is set to be 4×10^7 steps; thus, a time period over 2520 s can be simulated.

III. RESULTS AND DISCUSSION

A. Basic characteristic of a void during migration

To better understand the void migration behavior, we would like to first reveal the features of some physical quantities that are relevant to void migration. In Fig. 1, we depict the spatial distributions of the concentration field c_v, the mobility tensor component M_{11}, the temperature field T, and the vapor pressure P_{vap} at the beginning of migration of a circular void. The void is subjected to an unperturbed temperature gradient field along the horizontal x direction, with $\mathrm{d}T/\mathrm{d}x = 0.4\,\mathrm{K}/\mu\mathrm{m}$. The simulation cell size is $10\,\mu\mathrm{m} \times 5\,\mu\mathrm{m}$ and the void has a radius of $1\,\mu\mathrm{m}$. To obtain the quantities, the void is initially set with a sharp interface, and then an evolution over a time period of 6.3 s (i.e., 10^5 steps) is performed to recover the diffusive interface. Note that for such a short time period, the void migration is not significant. Moreover, due to the isotropic gradient energy and the short time period, the void maintains a circular shape, as can be clearly seen from the vacancy concentration field c_v shown in Fig. 1(a). The distribution of the mobility tensor component M_{11}, which is mainly relevant to the vacancy diffusion along the temperature gradient direction, clearly indicates that the diffusion is mainly confined to the void surface (i.e., the surface diffusion mechanism is dominant) and importantly, the diffusion is nonuniform along the surface. The tensor formula of surface diffusion has been included in the model in previous phase-field studies.[23,24] However, its effect on void migration behavior subjected to a temperature field, has not yet been revealed to the best of our knowledge. It is shown in this work that for a proper void size, such a surface diffusion flow can cause significant shape change and even interesting splitting behavior for voids under long time migration.

Distributions of the temperature field T and the vapor pressure P_{vap} inside the void are shown in Figs. 1(c) and 1(d), respectively. The profiles of temperature and vapor pressure along the center of line of the void are also shown

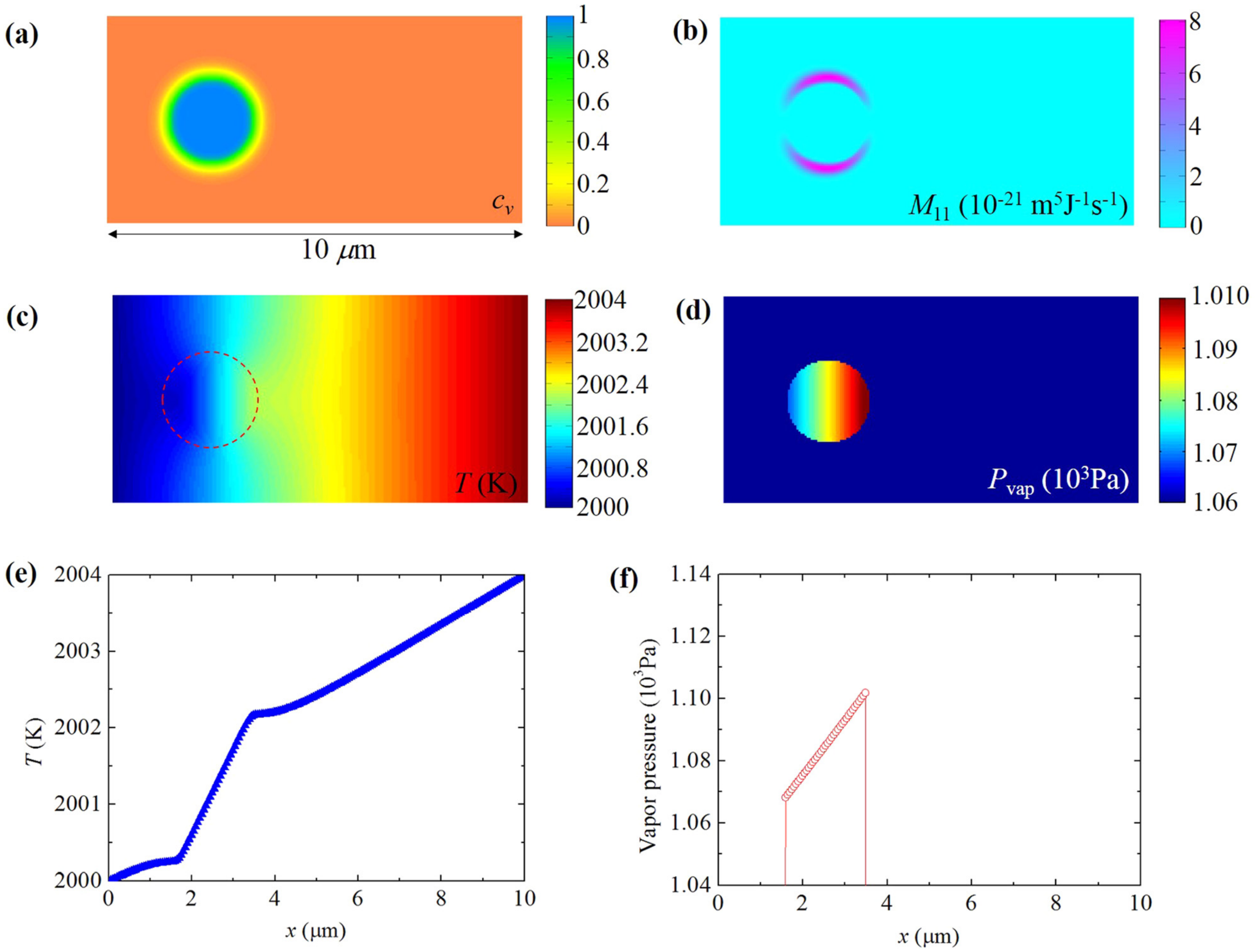

FIG. 1. Field distributions of a circular void (with a radius of $1\,\mu\mathrm{m}$) in the UO_2 matrix subjected to a temperature gradient field of $0.4\,\mathrm{K}/\mu\mathrm{m}$. (a) Vacancy concentration field c_v, (b) vacancy mobility component M_{11}, (c) temperature field T, and (d) vapor pressure P_{vap}. Profiles of the (e) temperature field and (f) vapor pressure along the center of line of the void.

in Figs. 1(e) and 1(f), respectively. It can be seen that there is an enhanced temperature gradient field inside the void due to the thermal conductivity difference between the void and the matrix. It is expected that the void has a larger migration velocity due to the enhanced temperature gradient field. The temperature gradient also causes a gradient of vapor pressure P_{vap} in the void [Figs. 1(d) and 1(f)]. One can see that the vapor pressure gradient is of about 2 Pa/μm. Although its value seems small, it is this vapor pressure gradient that drives void migration *via* the vapor transport mechanism, in which matrix species vaporize at the leading surface and condense at the trailing surface in the void.

Both the thermal transport mechanism and the vapor transport mechanism can contribute to void migration. To better see their importance, Figs. 2(a) and 2(b) respectively depict the atom flow density patterns caused by the two mechanisms, i.e., the thermal transport flow density $\mathbf{J}_T$, and the vapor transport flow density $\mathbf{J}_P$, at the beginning of migration of a circular void (with a radius of 1 μm) in the UO_2 matrix subjected to a temperature gradient field $\mathrm{d}T/\mathrm{d}x = 0.4$ K/μm. It can be seen that the thermal transport mechanism is mainly caused by the surface diffusion and the flow density $\mathbf{J}_T$ is along the void surface. Therefore, it can be regarded as an incompressible two phase flow along the interface between the void phase and the solid phase. It is worth noting that the flow density $\mathbf{J}_T$ is nonuniform along the void surface. $\mathbf{J}_T$ takes on much larger values at the top and bottom regions than at the left and right regions of the void surface. This is a result of the combined effect of the temperature gradient and the surface-dependent mobility tensor $\mathbf{M}$. In contrast with the thermal transport flow density $\mathbf{J}_T$, the vapor transport flow density $\mathbf{J}_P$ is along the temperature gradient direction and is rather uniform in the void due to the conservation of flow in the gas phase. Importantly, the maximum magnitude of the thermal transport flow density $\mathbf{J}_T$ is about two orders larger than that of the vapor transport flow density $\mathbf{J}_P$. It is expected that the thermal transport mechanism plays a much more important role than the vapor transport mechanism for small voids which have large surface-to-volume ratios. Only for voids with a typical width larger than 10 μm along the temperature gradient and an area larger than 100 μm^2, the vapor transport mechanism can be overwhelmed. The size of voids in this work lies in the regime where the thermal transport mechanism is dominant.

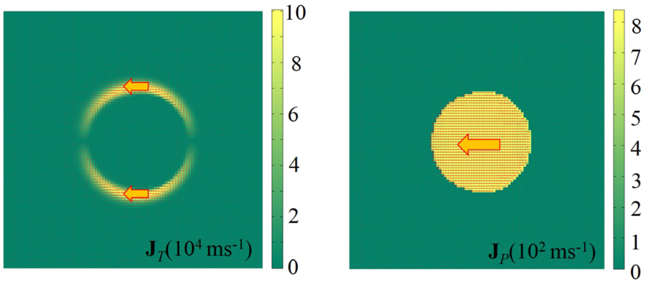

(a) (b)

FIG. 2. Atom flow patterns of the voids (with a radius of 1 μm) in the UO_2 matrix subjected to a temperature gradient field of 0.4 K/μm. (a) Thermal transport flow density $\mathbf{J}_T$ and (b) vapor transport flow density $\mathbf{J}_P$.

Now we investigate the long-time migration of circular voids. For a void of radius 0.5 μm and subjected to a temperature gradient field of $\sim$0.2 K/μm, the displacement of the void center as a function of time is depicted in Fig. 3(a). The insets also depict the distribution of the concentration field at $t = 0$ s and 252 s. The simulation cell size is taken to be 10 μm $\times$ 5 μm. It can be seen that the void migrates about 1.1 μm, and it maintains a circular shape during the migration. Except at the beginning due to the relaxation, the void migrates almost in a constant velocity of about 4.6 nm/s. The conservation of the concentration field is verified as shown in Fig. 3(b), where the lattice summation of the concentration field is traced as a function of time. The profiles of concentration field across the center of the void at $t = 0$ s and at $t = 252$ s are further shown in Figs. 3(c) and 3(d), respectively. It can be seen that the profile of concentration field is symmetric at the beginning, and it becomes asymmetric during the migration. Interestingly, a "tail" region, with a small but nonzero value of vacancy concentration, is left behind the void. Such a tail region is believed to be caused by the local unbalance between the flow caused by the temperature gradient (i.e., $\mathbf{J}_T + \mathbf{J}_P$), which drives the void surface to move, and the flow caused by the chemical potential $-\mathbf{M}\nabla\psi$, which tends to keep the vacancies inside the void. The appearance of a tail region indicates that the void trailing surface moves too fast to keep all the vacancies inside the void.

The effect of temperature gradient on the long-time migration of a circular void of radius 0.5 μm is further investigated. In Fig. 4, we depict the displacement of the void center as a function of time for a void subjected to an unperturbed temperature gradient of 0.2 K/μm or 0.4 K/μm. For comparison, besides the cases in which the matrix and the void have different thermal conductivities (i.e., $\kappa_{\mathrm{void}} = 0.2\ \kappa_{\mathrm{matrix}}$), we also present the cases in which the matrix and the void have the same thermal conductivity (i.e., $\kappa_{\mathrm{void}} = \kappa_{\mathrm{matrix}}$). The void migration velocity is almost proportional to the unperturbed temperature gradient. For example, the migration velocity is about 1.85 nm/s for the case $\mathrm{d}T/\mathrm{d}x = 0.2$ K/μm and $\kappa_{\mathrm{void}} = \kappa_{\mathrm{matrix}}$, whereas it increases to be 3.82 nm/s when the temperature gradient doubles. Moreover, the void migrates much faster (with almost two times the velocity) in the cases $\kappa_{\mathrm{void}} = 0.2\ \kappa_{\mathrm{matrix}}$ than that in the cases $\kappa_{\mathrm{void}} = \kappa_{\mathrm{matrix}}$.

B. Size-dependent void migration behavior

Now, we turn to the size effect on void migration. The migration of circular voids with different sizes in the UO_2 matrix subjected to the same temperature gradient field (i.e., 0.2 K/μm) is further simulated. The initial void radius is taken to be 0.5 μm, 0.75 μm, and 1.0 μm. Assume that the matrix and the void have different thermal conductivities (i.e., $\kappa_{\mathrm{void}} = 0.2\ \kappa_{\mathrm{matrix}}$). The snapshots of the concentration field during migration and displacement curves of the void center for various voids as a function of time are shown in Figs. 5(a) and 5(b), respectively. It can be seen that there is a slight change of shape for all the voids after migration. The final shape of the voids is slightly elliptical with a shorter

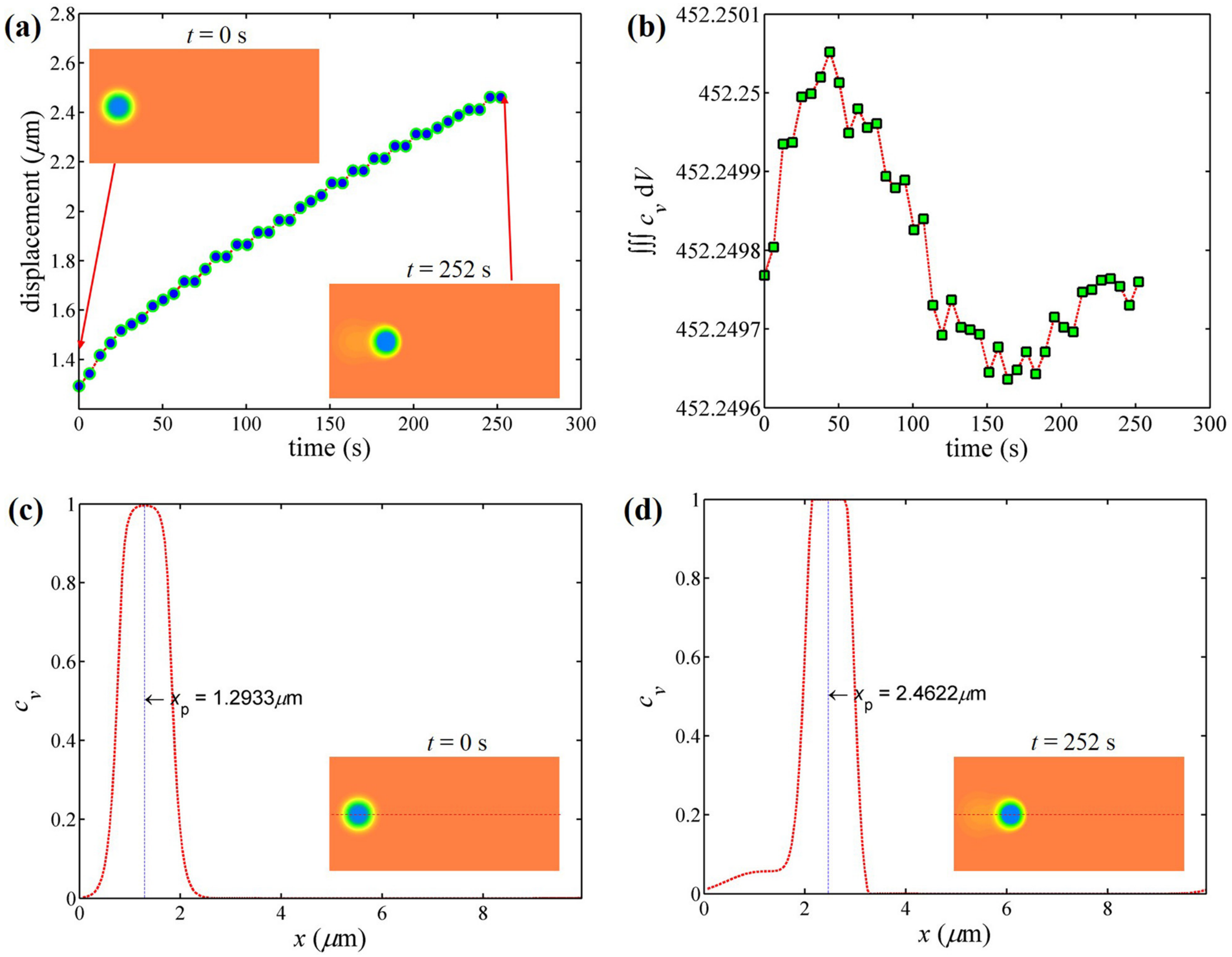

FIG. 3. Migration of a circular void (with a radius of 0.5 μm) in the UO$_2$ matrix subjected to a temperature gradient field of $\sim$0.2 K/μm. (a) Displacement of the void center as a function of time with the insets depicting the distribution of concentration field at $t = 0$ and 252 s, (b) lattice summation of the concentration field as a function of time, (c) concentration field profile across the center of the void (as indicated by the dash line in the inset) at $t = 0$ s, (d) concentration field profile across the center of the void (as indicated by the dash line in the inset) at $t = 252$ s.

width along the temperature gradient, indicating a larger velocity of the trailing surface than that of the leading surface at the beginning of migration. The larger the size of the void, the change of shape is more significant. Moreover, the void migration velocity decreases as the void radius increases. The migration velocity is about 4.6 nm/s, 3.5 nm/s, and 2.8 nm/s, for the voids with a radius of 0.5 μm, 0.75 μm, and 1.0 μm, respectively. That is, the void migration velocity is almost inversely proportional to the void size. According to analytical models,[29,31] the surface diffusion mechanism leads to an inversely proportional relation between the void migration velocity and the void size. Our result clearly indicates that the surface diffusion mechanism is dominant in the void migration. This result, together with those depicted in Figs. 3 and 4, shows that for small voids ($\leq$1 μm), the well-known characteristics of void migration (i.e., constant velocity, small change of shape, proportional to temperature gradient and inversely proportional to the void size) in consistence with analytical models can be recovered.

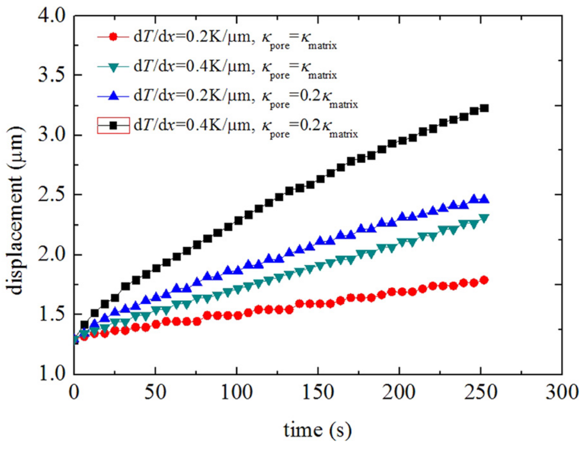

FIG. 4. Displacement of the void center as a function of time during the migration of (a) a circular void (with a radius of 0.5 μm) subjected to various temperature gradient fields.

The situation of large voids, however, is quite different. The long-time migration of a circular void (with a radius of 2 μm) subjected to a temperature gradient field of 0.4 K/μm is further simulated and the result is depicted in Fig. 6. From the snapshots of the concentration field distribution during the void migration, one can see that the void changes its shape significantly during the migration: first deforms into a cashew-like shape and eventually splits into two small voids.

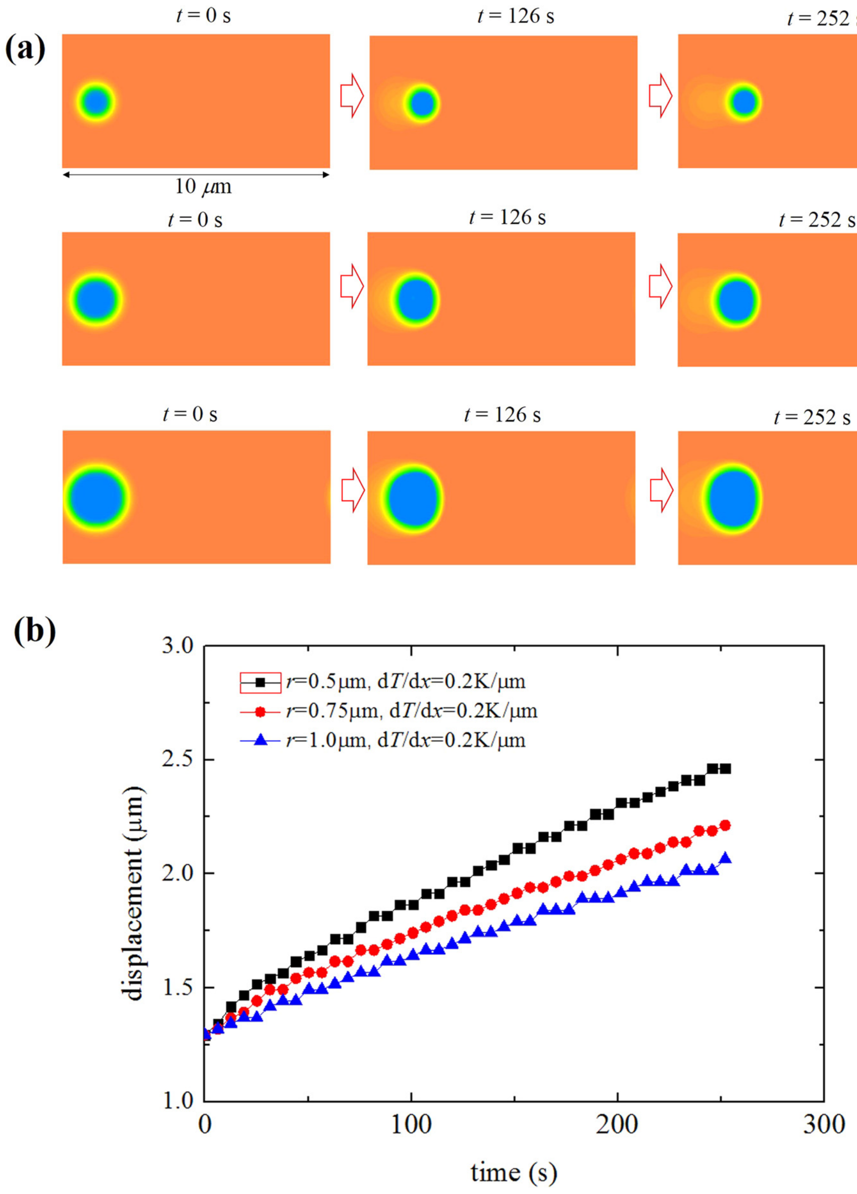

FIG. 5. (a) Snapshots during the migration of circular voids of radius 0.5 μm, 0.75 μm, and 1.0 μm subjected to a temperature gradient field of 0.2 K/μm. (b) Displacement of the void center as a function of time during the migration of the circular voids.

This is not found in the previous cases of migration behavior of small void sizes (≤ 1 μm). As already mentioned, the thermal transport flow density $\mathbf{J}_T$ is nonuniform along the void surface due to the combined effect of the temperature gradient and the surface-dependent mobility tensor $\mathbf{M}$. There are much larger values at the top and bottom regions than at the left and right regions of the void surface. Such a nonuniform flow density $\mathbf{J}_T$ leads to more significant material transport at the top and bottom region of the void than the middle region. As a consequence, the top and bottom regions of the void move ahead, and the middle region is left behind. Eventually, the void adopts a cashew-like shape, and finally even splits into two voids. For small voids, although the nonuniform flow density $\mathbf{J}_T$ also changes the shape of the void a little bit during the migration, the void can remain stable, due to the balance between the gradient energy (which tends to keep the void in circular shape) and the deformation brought by the surface diffusion. For voids with large enough sizes, the nonuniform flow density $\mathbf{J}_T$ changes the shape of the void significantly during the migration, and the void cannot remain stable, as the gradient energy is not enough to fight against the deformation brought by the surface diffusion. Note that the competitive effect between the gradient energy and the surface diffusion is not only a function of size but also a function of temperature gradient. The critical size of void splitting should be also dependent on the temperature gradient. Actually, even for small voids (≤ 1 μm), our simulation shows that by exerting a large enough temperature gradient (e.g., 1.5 K/μm, which may be unrealistic in practice), splitting can also be observed.

It is interesting to ask how the migration velocity of the void changes during the above complicated migration behavior shown in Fig. 6(a). To see this, in Fig. 6(b) we trace the displacement of the void as a function of time. Different from the previous cases, here, the displacement is represented by the rightmost edge point of the void(s) due to the shape change and splitting of the initial void. As labeled by capitals A to I, the snapshots shown in Fig. 6(a) have been indicated in the displacement curves. It can be seen that the migration velocity of the rightmost edge point of the void(s) exhibits a nonlinear feature. This might be mainly due to the fact that the rightmost edge point of the void(s) is not fixed

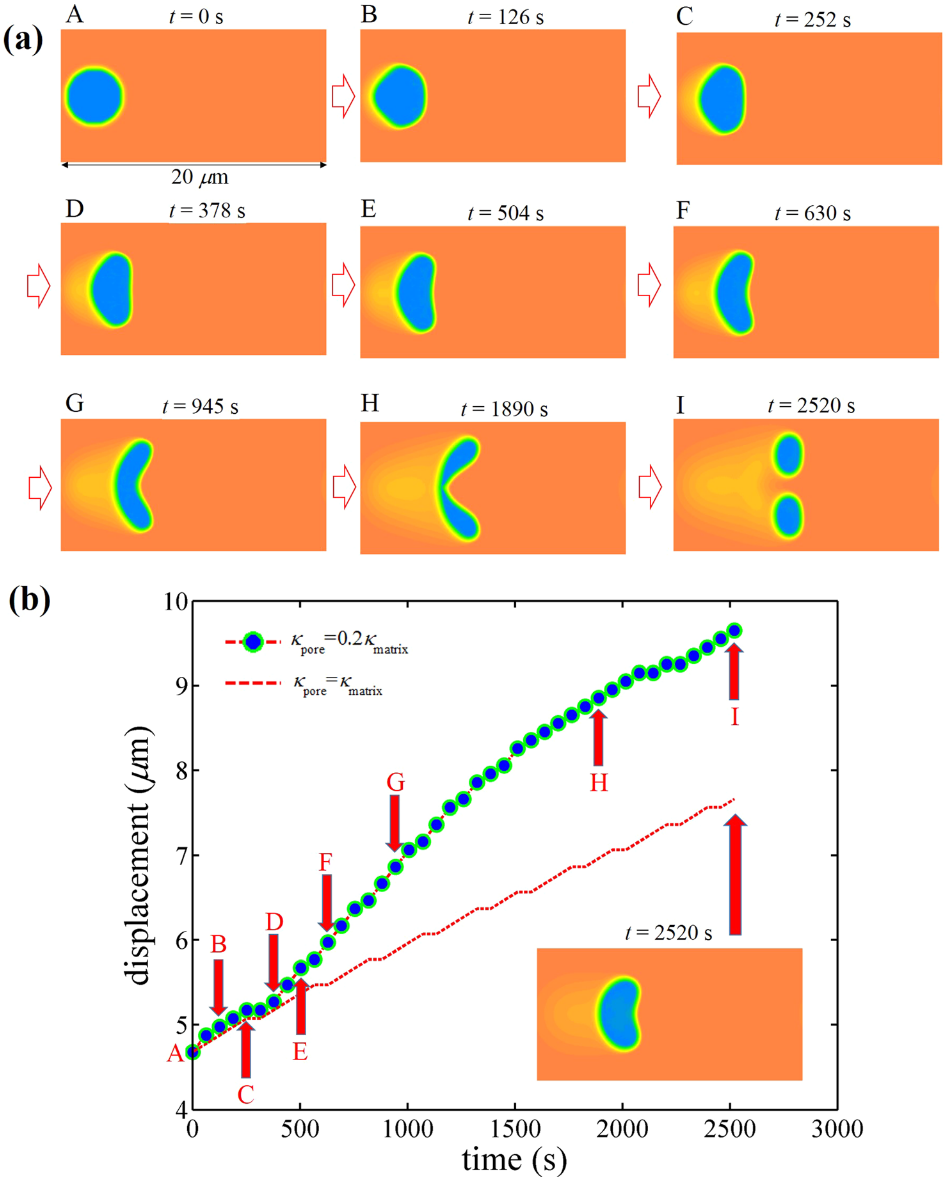

FIG. 6. (a) Snapshots during the migration of a circular void (with a radius of 2 μm) subjected to a temperature gradient field of 0.4 K/μm. The matrix and the void have different thermal conductivities (i.e., $\kappa_{\mathrm{void}} = 0.2\ \kappa_{\mathrm{matrix}}$). (b) The displacement of void as a function of time. For comparison, the case where the matrix and the void have the same thermal conductivity (i.e., $\kappa_{\mathrm{void}} = \kappa_{\mathrm{matrix}}$) is also depicted. The displacement is denoted by the rightmost edge of the void(s) due to the shape change and splitting of the void.

but changes during time. Anyway, after splitting, the void migration should be faster as the void size decreases. For comparison, we also depict the displacement of the void as a function of time in the case where the matrix and the void have the same thermal conductivity (i.e., $\kappa_{\mathrm{void}} = \kappa_{\mathrm{matrix}}$). In this case, as the temperature gradient experienced by the void is much smaller, the void does not split into two small voids after a migration time of 2520 s, and the displacement curve also exhibits a much more linear behavior than the previous case. Nevertheless, the deformation of the void into a cashew-like shape is also clearly seen, indicating it would also split into two small voids after a sufficiently long migration time. Our result thus shows that large voids subjected to a temperature gradient field are likely to exhibit significant shape change and even splitting after long-time migration.

C. Shape-dependent void migration behavior

It should be noted that, at equilibrium, the void should have a stable size and shape. Nevertheless, there are situations where the void initially has an unstable size and shape, for example, in fresh UO_2 samples under insufficient sintering treatment, or the working conditions of the UO_2 samples have been changed. After having an insight into the size-dependent void migration behavior, in the following, we explore how the initial shape of the void modifies the void migration.

In Fig. 7, we first depict the profiles of (a) the temperature field T and (b) the vapor pressure P_{vap} across the center line of three elliptical voids with different shapes in the UO_2 matrix subjected to an unperturbed temperature gradient of $dT/dx = 0.4$ K/μm. As indicated in the insets of Figs. 7(a) and 7(b), the elliptical voids have different values of the two elliptical axes, i.e., $(a, b) = (0.4\ \mu\mathrm{m}, 2.5\ \mu\mathrm{m})$, $(1\ \mu\mathrm{m}, 1\ \mu\mathrm{m})$, and $(2.5\ \mu\mathrm{m}, 0.4\ \mu\mathrm{m})$. Similar to the previous case of the circular void shown in Fig. 1, the voids are initially set with a sharp interface, and then an evolution over a time period of 6.3 s (i.e., 10^5 steps) is performed to recover the diffusive interface. The void migration and shape change are not significant over such a short time period. It can be seen that the void shape affects the distributions of the temperature field

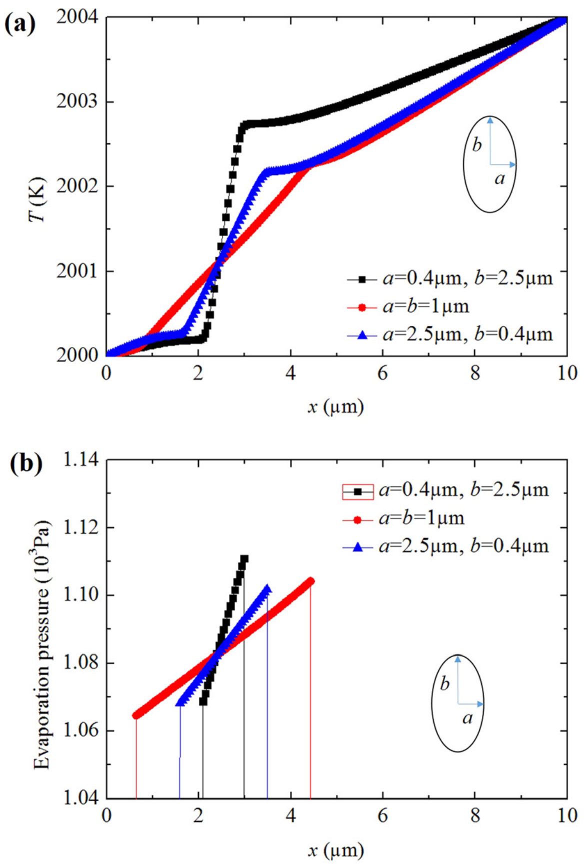

FIG. 7. Profiles of (a) temperature and (b) vapor pressure field across the center line of elliptical voids with different shapes subjected to an unperturbed temperature gradient of 0.4 K/μm. The elliptical voids have different values of the two elliptical axes, i.e., $(a, b) = (0.4\ \mu\text{m}, 2.5\ \mu\text{m})$, $(1\ \mu\text{m}, 1\ \mu\text{m})$, and $(2.5\ \mu\text{m}, 0.4\ \mu\text{m})$.

and the vapor pressure. As the void width along the temperature gradient i.e., a decreases, the temperature gradient increases remarkably inside the void while it decreases slightly in the matrix. The vapor pressure gradient inside the void also increases with the decrease of the void width along the temperature gradient.

The shape-dependent temperature field and vapor pressure profiles should modify the void migration. The shape-modifying effect on void migration is clearly indicated in the flow patterns at the beginning of migration for the three elliptical voids as shown in Fig. 8, where the thermal transport flow density $\mathbf{J}_T$ and the vapor transport flow density $\mathbf{J}_P$ are shown in Figs. 8(a) and 8(b), respectively. With the decrease of the void width, both the maximum magnitudes of $\mathbf{J}_T$ and $\mathbf{J}_P$ increase. Note that the area of surface that is parallel along the temperature gradient decreases with the decrease of the void width along the temperature gradient. The thermal transport becomes more localized and more significant change of the void shape during migration can be expected. Also due to the increase of the volume to surface ratio, the vapor transport mechanism could be more important with the decrease width of the void along the temperature gradient.

Having gained an insight into the relevant field distributions, now we simulate the long-time migration behavior of elliptical voids subjected to a temperature gradient field of 0.4 K/μm. We first consider three elliptical voids with the following values of the two elliptical axes: $(a, b) = (0.4\ \mu\text{m}, 2.5\ \mu\text{m})$, $(1\ \mu\text{m}, 1\ \mu\text{m})$, and $(2.5\ \mu\text{m}, 0.4\ \mu\text{m})$. That is, the size of the void is fixed to be $\pi\ \mu\text{m}^2$. Figure 9(a) depicts the snapshots of the concentration field c_v during the long-time migration of the three elliptical voids. It is found that the voids exhibit quite different shape relaxation behaviors at

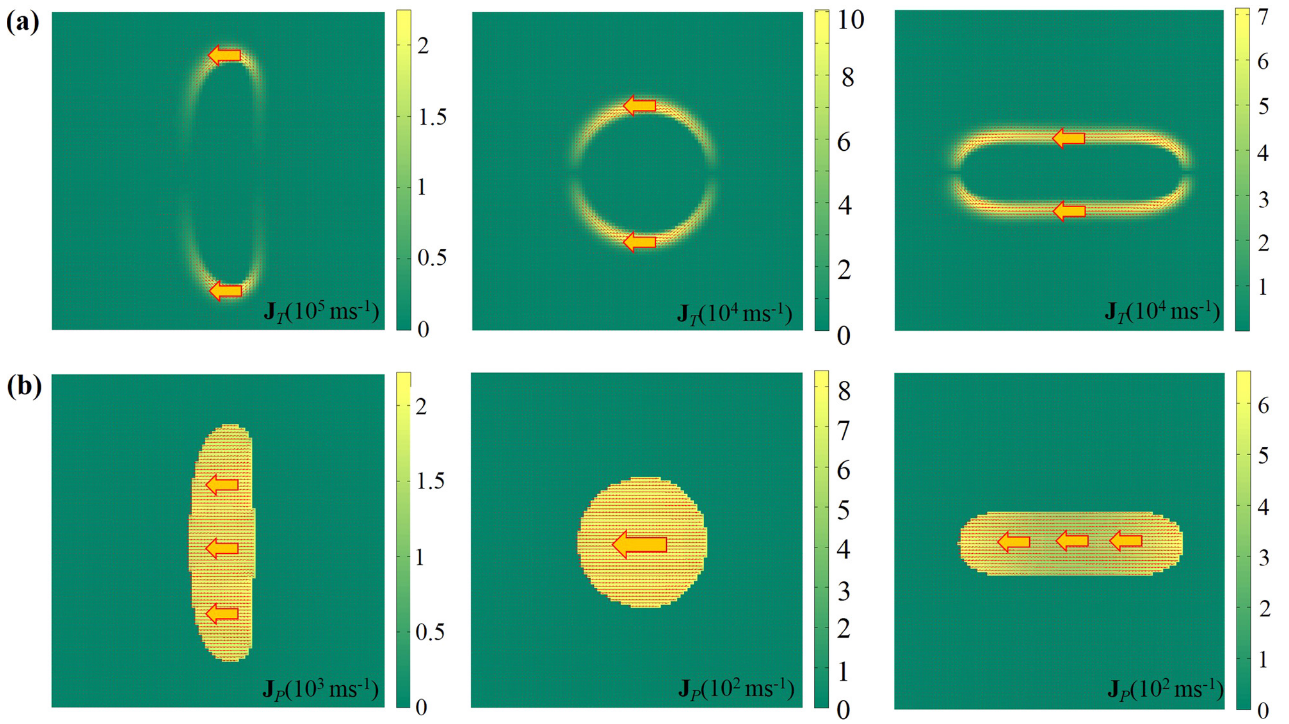

FIG. 8. Atom flow patterns of elliptical voids with different shapes subjected to an unperturbed temperature gradient of 0.4 K/μm. The voids have different values of the two elliptical axes, i.e., $(a, b) = (0.4\ \mu\text{m}, 2.5\ \mu\text{m})$, $(1\ \mu\text{m}, 1\ \mu\text{m})$, and $(2.5\ \mu\text{m}, 0.4\ \mu\text{m})$. (a) Thermal transport flow density $\mathbf{J}_T$ and (b) vapor transport flow density $\mathbf{J}_P$.

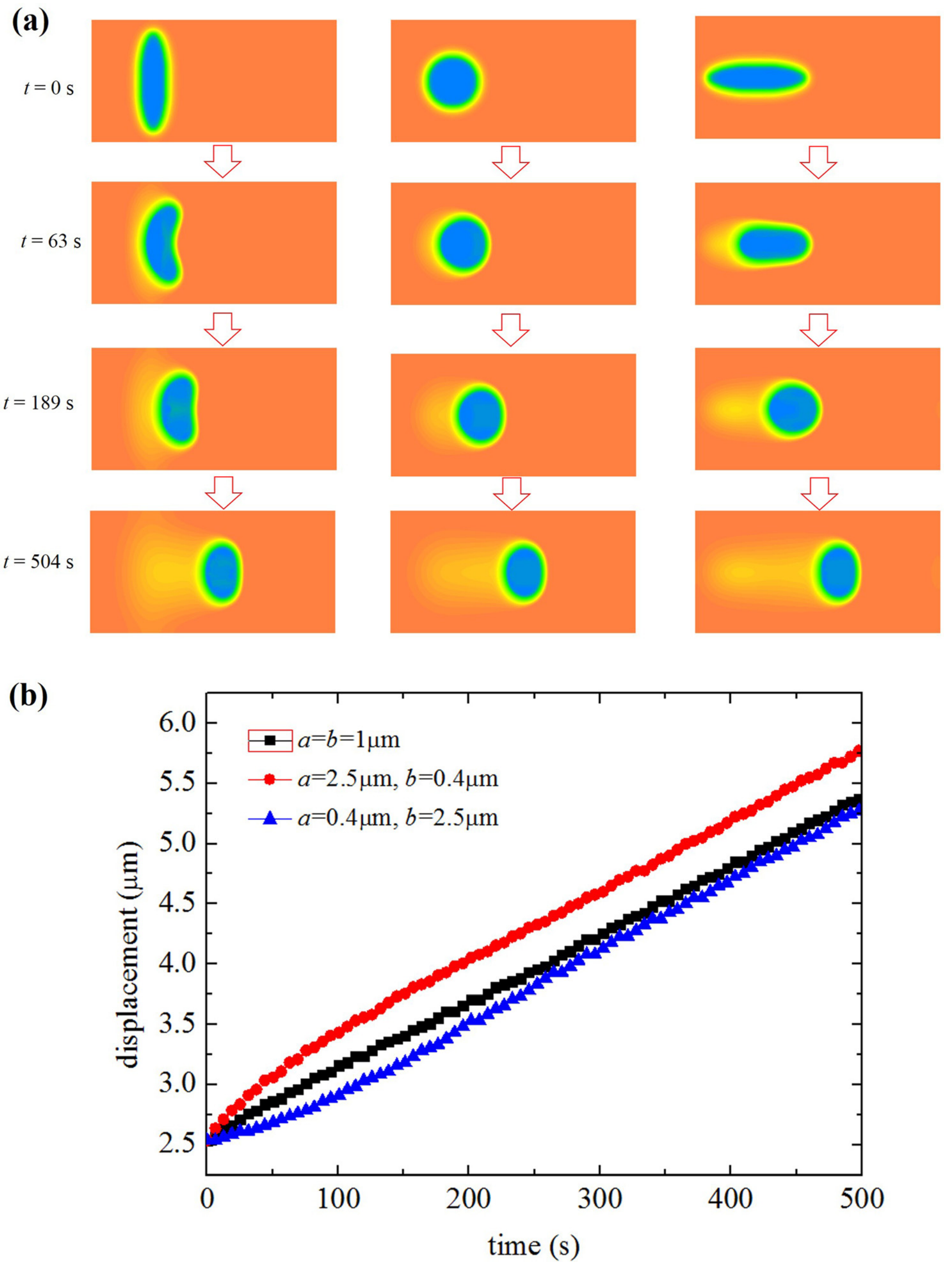

FIG. 9. (a) Snapshots during the migration of elliptical voids with different shapes subjected to a temperature gradient field of 0.4 K/μm. The voids have different values of the two elliptical axes, i.e., $(a, b) = (0.4\,\mu\text{m}, 2.5\,\mu\text{m})$, $(1\,\mu\text{m}, 1\,\mu\text{m})$, and $(2.5\,\mu\text{m}, 0.4\,\mu\text{m})$. (b) The displacement curves of the voids as a function of time. The displacement is denoted by the rightmost edge of the void(s) due to the shape change and splitting of the void.

the beginning of migration. A significant shape change is observed for the void with $(a, b) = (0.4\,\mu\text{m}, 2.5\,\mu\text{m})$ and for the void with $(a, b) = (2.5\,\mu\text{m}, 0.4\,\mu\text{m})$. The former deforms into a cashew-like shape, whereas the latter contracts along the temperature gradient. Despite the different shape relaxation, all the voids eventually adopt the same shape, which is slightly elliptical with $a < b$. No splitting of the voids is observed. The displacement curves of the voids as a function of time can be found in Fig. 9(b). Similar to the previous case, we trace the rightmost edge of the void(s) due to the shape change and splitting of the void. One can see that the void shape affects the void migration velocity. Due to the shape deformation at the beginning of migration, the migration velocity increases with the decrease of a. After the shape deformation, all the voids adopt the same shape, and they migrate with a similar velocity.

The result shown in Fig. 9 indicates that the size of the voids is not sufficiently large to cause splitting behavior, and the effect of the initial shape on void migration is gentle. The case is quite different for larger voids. To see this, we double the size of the three elliptical voids into $(a, b) = (0.8\,\mu\text{m}, 5\,\mu\text{m})$, $(2\,\mu\text{m}, 2\,\mu\text{m})$ and $(5\,\mu\text{m}, 0.8\,\mu\text{m})$, that is, the size of the void is fixed to be $4\pi\ \mu\text{m}^2$, and simulate their long-time migration behavior subjected to a temperature gradient field of 0.4 K/μm. The result is shown in Fig. 10, with Figs. 10(a) and 10(b) corresponding to the snapshots of the concentration field during the migration of voids, and the displacement curves of the voids as a function of time, respectively. At the beginning, the deformation behavior of each of the voids is quite similar to that found in small voids of the same shape shown in Fig. 9(a). However, the shape deformation is much slower for the large voids, and importantly, void splitting occurs after a sufficiently long time. For the void with $(a, b) = (0.8\,\mu\text{m}, 5\,\mu\text{m})$, it first deforms into a cashew-like shape and finally splits into two small voids at a time of about 2000 s. For the void with $(a, b) = (1\,\mu\text{m}, 1\,\mu\text{m})$, it also deforms into a cashew-like shape,

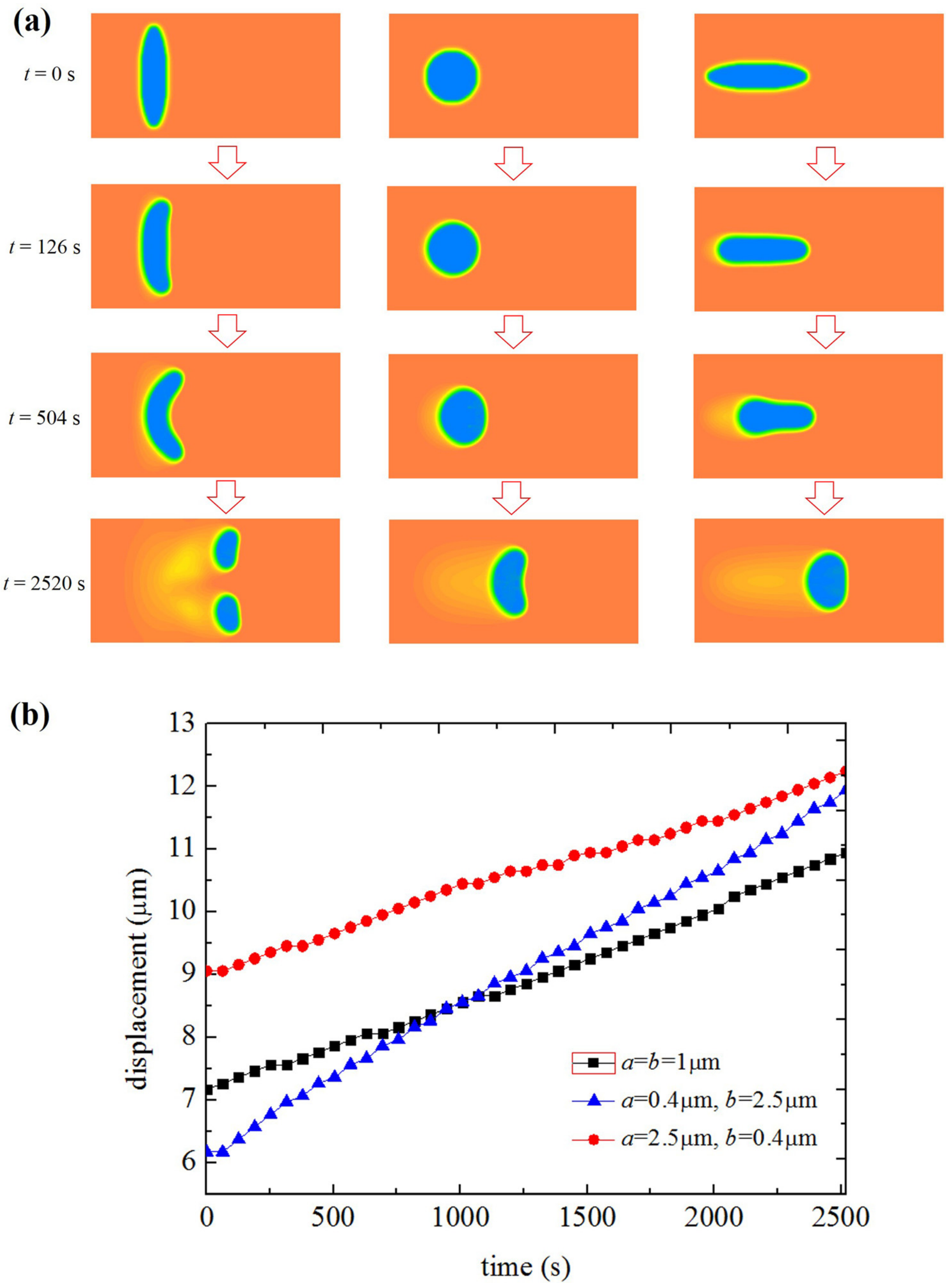

FIG. 10. (a) Snapshots during the migration of elliptical voids with different shapes subjected to a temperature gradient field of 0.4 K/μm. The voids have different values of the two elliptical axes, i.e., $(a,\ b) = (0.8\ \mu\text{m}, 5\ \mu\text{m})$, $(2\ \mu\text{m}, 2\ \mu\text{m})$, and $(5\ \mu\text{m}, 0.8\ \mu\text{m})$. (b) The displacement curves of the voids as a function of time. The displacement is denoted by the rightmost edge of the void(s) due to the shape change and splitting of the void.

but occurs in a much slow way. For void with $(a, b) = (5\ \mu\text{m}, 0.8\ \mu\text{m})$, it first contracts along the temperature gradient direction. Void splitting can be expected in the latter two voids but at a much longer of time than the first case, which is beyond the maximum time period of our simulation. After splitting, the small voids can maintain a stable size and shape, and eventually have a similar migration velocity, as that shown in Fig. 9. Therefore, the initial shape of the void modifies the migration velocity and the time point when splitting occurs (for large voids) at the beginning of migration due to the shape relaxation of the void. However, its effect on the long-time migration is minor.

D. Discussion

It is worth noting that lenticular voids with a typical width larger than 10 μm along the temperature gradient and an area larger than 100 μm^2 are often observed in UO_2 fuel rods in experiments.[30,32] While it is still not very clear on the exact picture of how a void evolves into a lenticular shape during its migration under the temperature gradient, it is generally accepted that lenticular voids are formed when the vapor transport mechanism is dominant. Actually, to capture the lenticular voids is also one of our motivations for developing a phase-field model with incorporating the vapor transport mechanism. Nevertheless, lenticular voids are not the focus points of this work. In this work, we aim to reveal novel void migration behaviors in conditions where the surface-diffusion mechanism is dominant over the vapor transport mechanism meanwhile the size of the void is large enough to overcome the interfacial energy to deform into non-circular shapes. The size of "large" voids we investigated (with an area of $\sim 10\ \mu\text{m}^2$) is still not large enough to show lenticular shapes. At this mediate size range, the void can be deformed during migration by the thermal diffusion flow rather than remaining in circular shape, however the flow is mainly caused by the surface-diffusion flow rather than the vapor transport flow. Below this mediate size range, the void migration is mainly caused by the surface-diffusion flow, but the void would tend to remain in the circular shape due to the large interfacial energy. Above this mediate size range, the diffusion flow is mainly caused by the vapor transport flow rather than the surface-diffusion flow and the void would be deformed into lenticular shapes.

For the void size range and at the temperature condition we investigated, the void deformation caused by the vapor transport flow is found to be much less important than that caused by the surface diffusion flow. The relatively weak effect of vapor transport flow density is not enough to cause the void to deform into lenticular shapes. Nevertheless, lenticular voids can indeed form when the void size is large enough as verified by our further simulation (not shown here). The lenticular shape is caused by the relative larger moving speed of the trailing surface than the leading surface due to the difference of vapor transport flow density at the two surfaces. This result is consistent with what has been found in a recent phase-field simulation work by Vance and Millett.[36]

It should be pointed out that our prediction is semi-qualitative. The simulations in this work are performed on a two dimensional mesh and based on the diffuse interface model. This might overestimate the surface-volume ratio and the importance of the surface diffusion mechanism, although the surface diffusion coefficient has been scaled [see, Eq. (12)]. We have examined that void splitting can still occur and the cashew-shaped voids can still appear if we keep the size of the void but decrease the surface diffusion flow density $\mathbf{J}_T$ by a factor of ten, or if we decrease the size of the void but increase the temperature gradient. This indicates that, once the surface diffusion is dominant and the void size is large enough to deform, this effect is quite universal. Moreover, useful information on the migration behavior of real three dimensional voids driven by a temperature gradient field can be inferred from our two dimensional simulation by geometry analysis. For example, similar shape change and splitting behavior can be expected along the transverse plane for cylindrical voids at a large size if their axis is perpendicular to the temperature gradient direction, whereas for spherical voids at a large size, the shape of the void would turn into a bowl-like shape and eventually into a toroidal shape with a hollow in the center. Note also that the migration behavior of voids in a solid found in this work is very alike to the migration behavior of an air bubble rising in water.[45] Actually, both these two phenomena belong to the migration behavior caused by incompressible two-phase flows. For an air bubble rising in a fluid, the two-phase flow is the air/fluid flow, where buoyancy and viscidity of the fluid play an important role. For the void migration in the solid, it is the atom flow along the interface of the void phase and the matrix phase that mainly causes the migration. Considering the similarity of the two phenomena, we believe that the novel void migration behavior revealed in this work can be found in porous solids at suitable conditions in experiment, especially in materials with a large temperature gradient (whose effect is analogous to buoyancy) and small interfacial energy (whose effect is analogous to viscidity).

IV. CONCLUSIONS

Based on an established phase-field model, simulations have been performed to reveal the effects of size and shape on the void migration behavior in a single crystal matrix subjected to a temperature gradient field. Several points have been improved in our phase-field model in comparison with the existing models in previous studies. First, it incorporates both the thermal transport flow and the vapor transport flow, with the temperature field and the vapor pressure appropriately solved. Second, the surface diffusion effect is treated by a tensorial formulation. Moreover, the interfacial energy and the coupling between the vacancy concentration field and the crystal order parameter field are carefully modeled. Simulations are applied to the UO_2 system. For small voids (with an area $\leq \pi\mu m^2$), the well-known characteristics of void migration (i.e., constant velocity, small change of shape, proportional to the temperature gradient and inversely proportional to the void size) in consistence with analytical models can be recovered. In contrast, for large voids (with an area of $\sim 10\ \mu m^2$), the voids change their shape significantly during migration, and eventually split into small voids, indicating that there is a size limit of the void below which it can remain stable under a temperature gradient field. Such a size-dependent behavior of void migration originates from the competitive effect of the interfacial energy and the surface diffusion flow. Moreover, the initial shape of the void modifies the migration velocity and the time point when splitting occurs at the beginning of migration due to the shape relaxation of the void, but has a minor effect on the long time migration. The migration behavior of voids found in this work is very alike to the other migration behaviors caused by incompressible two-phase flows.

ACKNOWLEDGMENTS

Helpful discussion with H. H. Wen is acknowledged. This work was supported by the National Key Basic Research Program of China (No. 2015CB351905) and the NSFC (Nos. 11474363, 11672339, 11602310, and 11232015). Yue Zheng also thanks support from the Special Program for Applied Research on Super Computation of the NSFC-Guangdong Joint Fund (the second phase), the Fok Ying Tung Foundation, the Guangdong Natural Science Funds for Distinguished Young Scholars, and the China Scholarship Council.

[1] C. S. Becquart, A. Souidi, C. Domain, M. Hou, L. Malerba, and R. E. Stoller, J. Nucl. Mater. **351**, 39–46 (2006).
[2] Y. Satoh, Y. Matsuda, T. Yoshiie, M. Kawai, H. Matsumura, H. Iwase, H. Abe, S. W. Kim, and T. Matsunaga, J. Nucl. Mater. **442**, S768–S772 (2013).
[3] B. Q. Fu, S. P. Fitzgerald, Q. Hou, J. Wang, and M. Li, Nucl. Instrum. Methods Phys. Res., Sect. B **393**, 169–173 (2017).
[4] R. E. Voskoboinikov and A. E. Volkov, J. Nucl. Mater. **297**, 262–270 (2001).
[5] H. Trinkaus and B. N. Singh, J. Nucl. Mater. **307**, 900–906 (2002).

[6] P. C. Millett, A. El-Azab, S. Rokkam, M. Tonks, and D. Wolf, Comput. Mater. Sci. **50**, 949–959 (2011).
[7] P. C. Millett, A. El-Azab, and D. Wolf, Comput. Mater. Sci. **50**, 960–970 (2011).
[8] Z. H. Xiao, A. A. Semenov, C. H. Woo, and S. Q. Shi, J. Nucl. Mater. **439**, 25–32 (2013).
[9] L. Zhang, M. R. Tonks, P. C. Millett, Y. Zhang, K. Chockalingam, and B. Biner, Comput. Mater. Sci. **56**, 161–165 (2012).
[10] J. B. Ainscough, F. Rigby, and S. C. Osborn, J. Nucl. Mater. **52**, 191–203 (1974).
[11] M. R. Tonks, Y. Zhang, X. Bai, and P. C. Millett, Mater. Res. Lett. **2**, 23–28 (2014).
[12] J. R. MacEwan and V. B. Lawson, J. Am. Ceram. Soc. **45**, 42–46 (1962).
[13] Y. F. Yin, R. G. Faulkner, and Z. Lu, J. Nucl. Mater. **389**, 225–232 (2009).
[14] C. Y. Yu, X. D. Xu, M. W. Chen, and C. T. Liu, J. Alloys Compd. **663**, 340–344 (2016).
[15] K. Lindgren, M. Boåsen, K. Stiller, P. Efsing, and M. Thuvander, J. Nucl. Mater. **488**, 222–230 (2017).
[16] R. Hargreaves and D. A. Collins, J. Br. Nucl. Energy Soc. **15**, 311–318 (1976).
[17] J. A. Turnbull, J. Nucl. Mater. **50**, 62–68 (1974).
[18] S. J. Zinkle and G. S. Was, Acta Mater. **61**, 735–758 (2013).
[19] A. G. Evans and R. W. Davidge, J. Nucl. Mater. **33**, 249–260 (1969).
[20] H. Matzke, Radiat. Eff. **53**, 219–242 (1980).
[21] D. R. De Halas and G. R. Horn, J. Nucl. Mater. **8**, 207–220 (1963).
[22] M. D. Freshley, D. W. Brite, J. L. Daniel, and P. E. Hart, J. Nucl. Mater. **62**, 138–166 (1976).
[23] K. Ahmed, C. A. Yablinsky, A. Schulte, T. Allen, and A. El-Azab, Modell. Simul. Mater. Sci. Eng. **21**, 065005 (2013).
[24] K. Ahmed, J. Pakarinen, T. Allen, and A. El-Azab, J. Nucl. Mater. **446**, 90–99 (2014).
[25] R. J. Brook, J. Am. Ceram. Soc. **52**, 56–57 (1969).
[26] S. B. Biner, Modell. Simul. Mater. Sci. Eng. **24**, 035019 (2016).
[27] P. G. Shewmon, Trans. Met. Soc. AIME **230**, 1134–1137 (1964).
[28] F. A. Nichols, J. Nucl. Mater. **22**, 214–222 (1967).
[29] F. A. Nichols, J. Nucl. Mater. **30**, 143–165 (1969).
[30] P. F. Sens, J. Nucl. Mater. **43**, 293–307 (1972).
[31] D. R. Olander, *Fundamental Aspects of Nuclear Reactor Fuel Elements: Solutions to Problems* (Department of Nuclear Engineering, California University, Berkeley, USA, 1976).
[32] H. Kawamata, H. Kaneko, H. Furuya, and M. Koizumi, J. Nucl. Mater. **68**, 48–53 (1977).
[33] T. G. Desai, P. Millett, M. Tonks, and D. Wolf, Acta Mater. **58**, 330–339 (2010).
[34] S. Y. Hu and C. H. Henager, Acta Mater. **58**, 3230–3237 (2010).
[35] Y. Li, S. Y. Hu, X. Sun, F. Gao, C. H. Henager, and M. Khaleel, J. Nucl. Mater. **407**, 119–125 (2010).
[36] I. W. Vance and P. C. Millett, J. Nucl. Mater. **490**, 299–304 (2017).
[37] L. Q. Chen, Annu. Rev. Mater. Res. **32**, 113–140 (2002).
[38] N. Provatas and K. Elder, *Phase-Field Methods in Materials Science and Engineering* (John Wiley & Sons, 2011).
[39] K. Ahmed, T. Allen, and A. El-Azab, J. Mater. Sci. **51**, 1261–1277 (2016).
[40] K. Ahmed, M. Tonks, Y. Zhang, B. Biner, and A. El-Azab, Comput. Mater. Sci. **134**, 25–37 (2017).
[41] M. J. F. Notley and I. J. Hastings, Nucl. Eng. Des. **56**, 163–175 (1980).
[42] P. S. Maiya, J. Nucl. Mater. **40**, 57–65 (1971).
[43] B. E. Poling, J. M. Prausnitz, and J. P. O'connell, *The Properties of Gases and Liquids* (McGraw-Hill, New York 2001).
[44] J. Belle, J. Nucl. Mater. **30**, 3–15 (1969).
[45] M. Sussman, A. S. Almgren, J. B. Bell, P. Colella, L. H. Howell, and M. L. Welcome, J. Comput. Phys. **148**, 81–124 (1999).